ELSEVIER

Advances in Engineering Software 35 (2004) 585–591

ADVANCES IN ENGINEERING SOFTWARE

www.elsevier.com/locate/advengsoft

Short communication

A modified isoparametric mapping fill method to display color mapping of data

Ke-Yong Wang[a], Qing-Hua Qin[a,b,*], Yi-Lan Kang[a]

[a]*Department of Mechanics, School of Mechanical Engineering, Tianjin University, Tianjin, 300072, China*
[b]*Department of Engineering, Faculty of Engineering and Information Technology, Australian National University, Engineering Building 32, North Road, Canberra, ACT 0200, Australia*

Received 23 January 2004; revised 27 May 2004; accepted 18 June 2004

Abstract

This work presents a reliable and efficient technique for displaying color mapping of data for post-processing of the Hybrid-Trefftz (HT) finite element method (FEM). The isoparametric mapping fill method developed in conventional FE models is generalized to HT FE models. Several steps of the procedure for HT FEM are demonstrated, as well as the aspects to be modified. For illustration purposes, a computer program has been written in VC++ and two 2D examples discretized by HT FEM are provided. The results are found to agree well with the analytical solutions although there are some discrepancies. Finally, conclusions are inferred and extension of this work to the 3D case is discussed.

Keywords: Conventional finite element method; Hybrid-Trefftz finite element method; Modified isoparametric mapping fill method; ABAQUS; Contour

1. Introduction

The conventional finite element method (FEM) is a numerical technique which is suitable for solving complex problems in science and engineering through a discretization process. One of the advantages of this method is that it can be explained through physical concepts and hence is most appealing to engineers and researchers. However, it has been found that conventional FEM is not efficient for certain special problems including local flaws, unless the density of the corresponding FEM mesh is significantly increased near the local effect region. In contrast, Hybrid-Trefftz (HT) FEM, introduced by Jirousek and Leon [1] about 20 years ago, can handle most local singularity problems without troublesome mesh refinement. In particular, two main advantages stem from the HT FE model [1,2]: firstly, the elemental formulation calls for integration along the element boundaries only and, secondly, problems with singularities or infinite domains can be easily treated, provided exact local solutions are available. Therefore, developing contouring algorithms and cloud-data schemes associated with HT FEM is of great interest.

With the rapid development of computer graphic techniques, the pre- and post-processing functions of FEM codes have become more and more realizable and important in numerical analysis of engineering problems. Up to now, although excellent visualization functions exist in some commercial finite element software such as ABAQUS, these visualization tools are limited to the software itself. Recently, the authors have coded an ABAQUS 6.2 user-defined element subroutine based on HT FEM. Because plotting of user elements is not supported in ABAQUS/Viewer, cloud data between contour lines cannot be displayed, so it is not convenient to evaluate deformed field information visually and quickly in the maintenance of data. In view of this, it is essential to develop a graphic representation function which is applicable to user-defined elements, as a supplement to conventional visualization software.

Over the past few decades, a number of procedures for generating cloud data have been reported. Stelzer and

* Corresponding author. Address: Department of Engineering, Faculty of Engineering, Information Technology, The Australian National University, Engineering building 32, North Road, Canberra, ACT 0200, Australia. Tel.: +61-2-6125-8274; fax: +61-2-6125-0506.
E-mail address: qinghua.qin@anu.edu.au (Q.-H. Qin).

0965-9978/$ - see front matter © 2004 Elsevier Ltd. All rights reserved.
doi:10.1016/j.advengsoft.2004.06.009

Welzel [3] compared the performance of three techniques: (a) linear approximations with subelement regions [4]; (b) a method starting from a point and moving stepwise along the tangent of the contour to an adjacent point [5,6]; (c) a method covering a finite element mesh with a second triangularization mesh in which a linear interpolation is used [7]. Subsequently, Lima and Soriano [8] presented a combination of the first and second methods. Studies reported in Refs. [9–12] developed a series of approaches, such as an algorithm based on quadrilateral mesh, to generate high quality cloud data. More recent work in this direction can be found in Refs. [13–16]. Studies in Refs. [13,14] employed the so-called direct fill method which needs to distinguish the points of intersection between scanning lines and element edges. The cloud data generated in Ref. [14] depends strongly on contours. The technique given in Ref. [15] is based on dividing higher-order surfaces into triangles. In this paper, some modifications of the isoparametric mapping fill method (IMFM) [16] have been made in order to make it suitable for HT FE models. Because the modified IMFM is independent of element shapes and of contours, the proposed algorithm seems promising for analyzing engineering problems with ABAQUS-based HT FEM.

2. Display of cloud data in the HT FE model

2.1. The theory of two-dimensional HT FEM

In this subsection, the outline of HT FEM presented in Refs. [17,18] is briefly reviewed for the sake of completeness.

The governing equations of plane elasticity may be summarized as follows

$$\mathbf{L}^{\mathrm{T}}\boldsymbol{\sigma}+\bar{\mathbf{b}}=0 \quad \text{on } \Omega \tag{1a}$$

$$\boldsymbol{\sigma}=\mathbf{D}\boldsymbol{\varepsilon} \quad \text{on } \Omega \tag{1b}$$

$$\boldsymbol{\varepsilon}=\mathbf{L}\mathbf{u} \quad \text{on } \Omega \tag{1c}$$

together with

$$\mathbf{u}=\bar{\mathbf{u}} \quad \text{on } \Gamma_u \tag{1d}$$

and

$$\mathbf{t}=\mathbf{A}\boldsymbol{\sigma}=\bar{\mathbf{t}} \quad \text{on } \Gamma_t \tag{1e}$$

where

$$\mathbf{L}=\begin{bmatrix} \dfrac{\partial}{\partial x} & 0 \\ 0 & \dfrac{\partial}{\partial y} \\ \dfrac{\partial}{\partial y} & \dfrac{\partial}{\partial x} \end{bmatrix} \tag{2a}$$

$$\mathbf{D}=\frac{E_0}{1-\nu_0^2}\begin{bmatrix} 1 & \nu_0 & 0 \\ \nu_0 & 1 & 0 \\ 0 & 0 & \dfrac{1-\nu_0}{2} \end{bmatrix} \tag{2b}$$

$$\mathbf{A}=\begin{bmatrix} n_x & 0 & n_y \\ 0 & n_y & n_x \end{bmatrix} \tag{2c}$$

$E_0=E$, $\nu_0=\nu$ for plane stress problems, and
$E_0=E/(1-\nu^2)$, $\nu_0=\nu/(1-\nu)$ for plane strain problems.

Ω designates the domain under consideration, Γ_u and Γ_t ($\partial\Omega=\Gamma_u\cup\Gamma_t$) stand for the parts of the boundary on which displacements and tractions are specified, respectively, n_x, n_y are direction cosines of the external normal at a given point on the boundary, and E, ν stand for the Young's modulus and the Poisson's ratio of the material, respectively.

The HT FE model assumes the following two independent displacement fields on each element subdomain Ω_e [18]:

(1) a non-conforming intra-element Trefftz field given by (see Fig. 1)

$$u_e=\breve{\mathbf{u}}_e+\sum_{j=1}^{m}\boldsymbol{\Phi}_j c_j=\breve{\mathbf{u}}_e+\boldsymbol{\Phi}_e\mathbf{c}_e \tag{3}$$

where m is the number of fundamental solutions, c_j are undetermined coefficients and $\breve{\mathbf{u}}_e$ and $\boldsymbol{\Phi}_j$ are, respectively, the particular and homogeneous solutions to the governing differential equations (1a)–(1c). In the presence of constant body forces $\bar{b}$, the particular solution is conveniently taken as

$$\breve{\mathbf{u}}_e=\frac{1+\nu_0}{E_0}\begin{Bmatrix} \bar{b}_x y^2 \\ \bar{b}_y x^2 \end{Bmatrix} \tag{4}$$

(2) an exactly and minimally conforming auxiliary displacement field (see Fig. 1)

$$\tilde{\mathbf{u}}_e=\tilde{\mathbf{N}}_e\mathbf{d}_e \tag{5}$$

is independently assumed along the element boundary ($\tilde{\mathbf{N}}_e$ here is the matrix of conventional FE shape functions) in terms of the element nodal displacement vector in the global coordinate system $\mathbf{d}_e$.

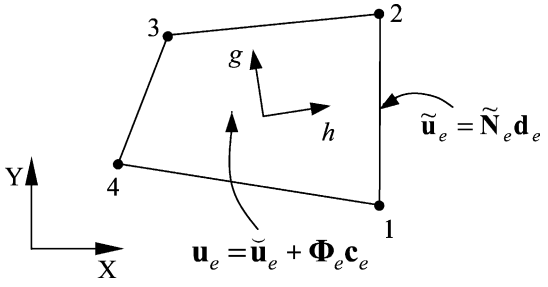

Fig. 1. Typical HT 4-node element (C2D4T) with two independent displacement fields.

The corresponding stress field of the element

$$\boldsymbol{\sigma}_e = \breve{\boldsymbol{\sigma}}_e + \sum_{j=1}^{m} \boldsymbol{\Psi}_j c_j = \breve{\boldsymbol{\sigma}}_e + \boldsymbol{\Psi}_e \mathbf{c}_e \tag{6}$$

is readily obtained by setting $\boldsymbol{\sigma}_e = \mathbf{D}\mathbf{L}\mathbf{u}_e$, where again for constant body forces

$$\breve{\boldsymbol{\sigma}}_e = \begin{Bmatrix} 0 \\ 0 \\ \bar{b}_x y + \bar{b}_y x \end{Bmatrix} \tag{7}$$

Using Eqs. (6) and (7), the boundary tractions $\mathbf{t}_e$ can be given in the form

$$\mathbf{t}_e = \mathbf{A}\boldsymbol{\sigma}_e = \breve{\mathbf{t}}_e + \boldsymbol{\Theta}_e \mathbf{c}_e \tag{8}$$

where

$$\breve{\mathbf{t}}_e = \mathbf{A}\breve{\boldsymbol{\sigma}}_e, \quad \boldsymbol{\Theta}_e = \mathbf{A}\boldsymbol{\Psi}_e \tag{9}$$

The HT FE formulation for plane elasticity can be derived by way of the functional [17]

$$\Pi_m(\mathbf{u}, \tilde{\mathbf{u}}) = \sum_e \Pi_{\mathrm{me}} = \sum_e \left[\iint_{\Omega_e} \frac{1}{2} \boldsymbol{\sigma}^{\mathrm{T}} \mathbf{C} \boldsymbol{\sigma} \, \mathrm{d}\Omega - \int_{\Gamma_{eu}} \mathbf{t}\bar{\mathbf{u}} \, \mathrm{d}\Gamma - \int_{\Gamma_{et}} (\mathbf{t} - \bar{\mathbf{t}})\tilde{\mathbf{u}} \, \mathrm{d}\Gamma - \int_{\Gamma_{eI}} \mathbf{t}\tilde{\mathbf{u}} \, \mathrm{d}\Gamma \right] \tag{10}$$

where the matrix $\mathbf{C} = \mathbf{D}^{-1}$ as well as Eq. (1a) are assumed to be satisfied, a priori.

The boundary Γ_e of a particular element consists of the following parts

$$\Gamma_e = \Gamma_{eu} \cup \Gamma_{et} \cup \Gamma_{eI} \tag{11}$$

where

$$\Gamma_{eu} = \Gamma_u \cap \Gamma_e \tag{12a}$$

$$\Gamma_{et} = \Gamma_t \cap \Gamma_e \tag{12b}$$

and Γ_{eI} is the inter-element boundary.

Applying a series of derivations to Eq. (10) yields the customary force–displacement relationship

$$\mathbf{K}_e \mathbf{d}_e = \mathbf{P}_e \tag{13}$$

where

$$\mathbf{K}_e = \mathbf{G}_e^{\mathrm{T}} \mathbf{H}_e^{-1} \mathbf{G}_e \tag{14a}$$

$$\mathbf{P}_e = \mathbf{G}_e^{\mathrm{T}} \mathbf{H}_e^{-1} \mathbf{r}_{1e} - \mathbf{r}_{2e} \tag{14b}$$

$$\mathbf{H}_e = \int_{\Gamma_e} \boldsymbol{\Theta}_e^{\mathrm{T}} \boldsymbol{\Phi}_e \, \mathrm{d}\Gamma = \int_{\Gamma_e} \boldsymbol{\Phi}_e^{\mathrm{T}} \boldsymbol{\Theta}_e \, \mathrm{d}\Gamma \tag{14c}$$

$$\mathbf{G}_e = \int_{\Gamma_e} \boldsymbol{\Theta}_e^{\mathrm{T}} \tilde{\mathbf{N}}_e \, \mathrm{d}\Gamma \tag{14d}$$

$$\mathbf{r}_{1e} = \int_{\Gamma_e} \boldsymbol{\Theta}_e^{\mathrm{T}} \breve{\mathbf{u}}_e \, \mathrm{d}\Gamma \tag{14e}$$

$$\mathbf{r}_{2e} = \int_{\Gamma_e} \tilde{\mathbf{N}}_e^{\mathrm{T}} \breve{\mathbf{t}}_e \, \mathrm{d}\Gamma - \int_{\Gamma_{et}} \tilde{\mathbf{N}}_e^{\mathrm{T}} \bar{\mathbf{t}}_e \, \mathrm{d}\Gamma \tag{14f}$$

$$\mathbf{c}_e = -\mathbf{H}_e^{-1} \mathbf{r}_{1e} + \mathbf{H}_e^{-1} \mathbf{G}_e \mathbf{d}_e \tag{14g}$$

$\mathbf{K}_e$ and $\mathbf{P}_e$ stand for the element stiffness matrix and the element equivalent nodal load vector, respectively, and $\mathbf{H}_e$ is the element flexibility matrix.

The global stiffness matrix equation is obtained by the assembly of Eq. (13) for all individual elements. It should be noted that the internal displacements $\mathbf{u}_e$ are, however, in error by discarding three rigid-body motion modes. But these lacking terms can easily be recovered by setting for the augmented internal displacements

$$\mathbf{u}_e = \breve{\mathbf{u}}_e + \boldsymbol{\Phi}_e \mathbf{c}_e + \bar{\boldsymbol{\Phi}}_e \bar{\mathbf{c}}_e \tag{15}$$

with

$$\bar{\boldsymbol{\Phi}}_e = \begin{bmatrix} 1 & 0 & y \\ 0 & 1 & -x \end{bmatrix} \tag{16}$$

and using a least-square procedure to match with the nodal displacements $\{\tilde{u}_i, \tilde{v}_i\}^{\mathrm{T}}$ at corner nodes leads to

$$\bar{\mathbf{c}}_e = \mathbf{R}_e^{-1} \mathbf{r}_e \tag{17}$$

where

$$\mathbf{R}_e = \sum_{i=1}^{n} \begin{bmatrix} 1 & 0 & y_i \\ 0 & 1 & -x_i \\ y_i & -x_i & (x_i^2 + y_i^2) \end{bmatrix} \tag{18a}$$

$$\mathbf{r}_e = \sum_{i=1}^{n} \begin{Bmatrix} \tilde{u}_i - u_i \\ \tilde{v}_i - v_i \\ (\tilde{u}_i - u_i) y_i - (\tilde{v}_i - v_i) x_i \end{Bmatrix} \tag{18b}$$

in which n stands for number of nodes on the element.

2.2. The modified isoparametric mapping fill method

With the concept of isoparametric elements [16], the trial functions are not taken in a general quadrilateral domain but in a unit square, which is the suitable mapped element domain. Here, we can still imitate this method. Conventional FEM employs a natural coordinate system whose ξ and η both range from -1 to $+1$, whereas HT FEM adopts an alternative non-dimensional system in which h and g can

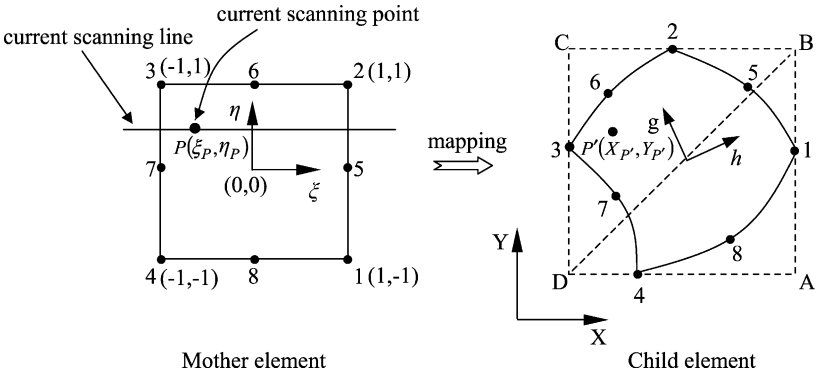

Fig. 2. Scanning region of HT 8-node quadrilateral element (C2D8T).

be written as

$$h = \frac{x}{a} \tag{19a}$$

$$g = \frac{y}{a} \tag{19b}$$

where

$$a = \frac{1}{n}\sum_{i=1}^{n}\sqrt{x_i^2 + y_i^2} \tag{20}$$

$$x = X - X_c \tag{21a}$$

$$y = Y - Y_c \tag{21b}$$

x, y stand for the local coordinate system which originates at the element centroid, a is the average distance between the element centroid and its nodes, and X_c, Y_c are the global coordinates of the element centroid. Only by using this non-dimensional coordinate system can we prevent the element stiffness matrix $\mathbf{K}_e$ from singularity and from overflow.

In conventional FEM, the following formulations exist

$$X = \sum_{i=1}^{n} N_i(\xi,\eta)X_i \tag{22a}$$

$$Y = \sum_{i=1}^{n} N_i(\xi,\eta)Y_i \tag{22b}$$

where $N_i(\xi,\eta)$ are shape functions, (X_i,Y_i) and F_i are the global coordinates and field variables of the element, respectively.

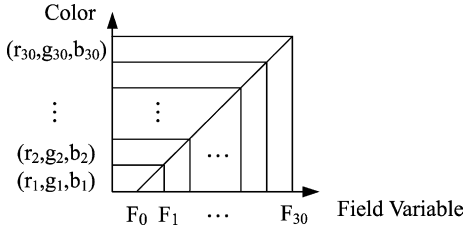

Fig. 3. Relationship between field variable and color.

The steps of the fill procedure based on modified IMFM are described in subsequent subsections.

2.2.1. Relationship between mother and child elements

A regular element (mother element) in the natural coordinate system (ξ,η) can be readily transformed to a distorted one (child element) in the global coordinate system (X,Y). In order to apply IMFM to HT FE model, we must also construct a relation between the two coordinate systems (ξ,η) and (h,g) which can be summarized as follows:

$$\left\{\begin{matrix}\xi\\ \eta\end{matrix}\right\} \Rightarrow \left\{\begin{matrix} X = \sum_{i=1}^{n} N_i(\xi,\eta)X_i \\ Y = \sum_{i=1}^{n} N_i(\xi,\eta)Y_i \end{matrix}\right\} \Rightarrow \left\{\begin{matrix} h = \dfrac{X - X_c}{a} \\ g = \dfrac{Y - Y_c}{a} \end{matrix}\right\} \tag{23}$$

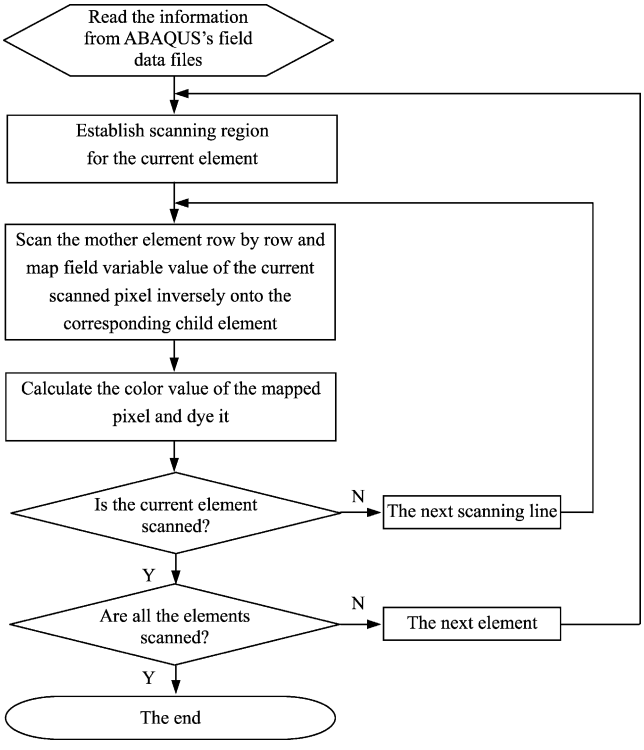

Fig. 4. Flow chart of the modified isoparametric mapping fill algorithm.

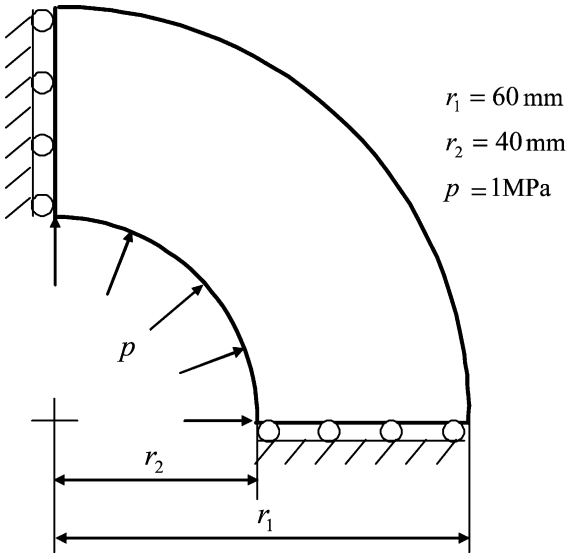

Fig. 5. Quarter of a hollow cylinder subjected to internal pressure.

The meaning of above relation may be illustrated in Fig. 2. For example, once the natural coordinates of a point $P(\xi_P,\eta_P)$ within the mother element are given, the global coordinates of corresponding mapped point $P'(X_{P'},Y_{P'})$ within the child element can be easily calculated by means of the second expression of Eq. (23). Subsequently, using the right-hand side of formulations of Eq. (23) one can transform the global coordinates $(X_{P'},Y_{P'})$ of point P' into the non-dimensional ones $(h_{P'},g_{P'})$. Now the field value at this point can be obtained with the aid of Eqs. (5), (6) and (15). Thus, the relationship between mother and child elements is linked in a simple way.

2.2.2. Construction of scanning region for the element

Child elements in arbitrary directions can be mapped onto the same mother element. The key issue in this mapping process is the determination of the number of scanning points in the mother element. In this paper, the maximum scanning region principle presented in Ref. [16] is employed to determine the number of scanning points. The principle is briefly described here for the readers' convenience. By the principle, we mean that it starts with calculating the rectangular frame containing the child element (see the square formed by dotted line in Fig. 2); then, the number of scanning points along ξ and η on the mother element are determined according to the distance between two catercorner points of this frame (for example, BD in Fig. 2). In practice, we set the number of scanning points to be the number of pixels along the catercorner line.

2.2.3. Relationship between field variable and color

The choice of color is important in achieving the desired visualization effect of the data field. With VC++, we have a color setting function, COLORREF RGB(BYTE bRed, BYTE bGreen, BYTE bBlue), which has three parameters. All the three parameters vary from 0 to 255, so that 256^3 colors [19] can be obtained. Therefore, 30 colors, gradually changing from yellow to blue and white by adjusting these three parameters, are selected carefully. Generally, the relationship between field variable and color is determined according to the following rule: the smaller the field variable, the lighter the color, and the bigger, the darker. As illustrated in Fig. 3, we divide the data field into a certain number of zones, each of which corresponds to a color value.

2.3. Flow chart of the modified isoparametric mapping fill algorithm for HT FEM

To investigate the performance of the modified isoparametric mapping fill algorithm, a computer program with VC++ was written, with all real variables set to be in

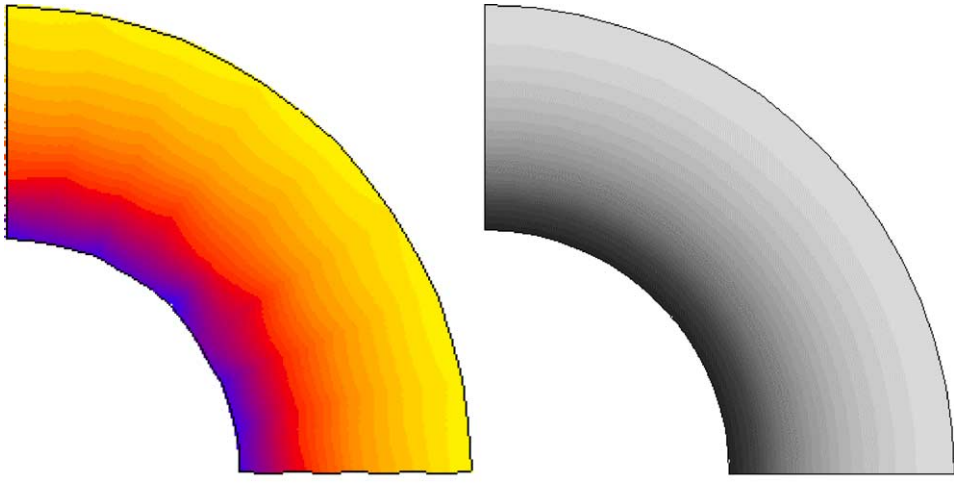

(a) Modified IMFM solution (b) Analytical solution

Fig. 6. Cloud data of Mises equivalent stress for the hollow cylinder.

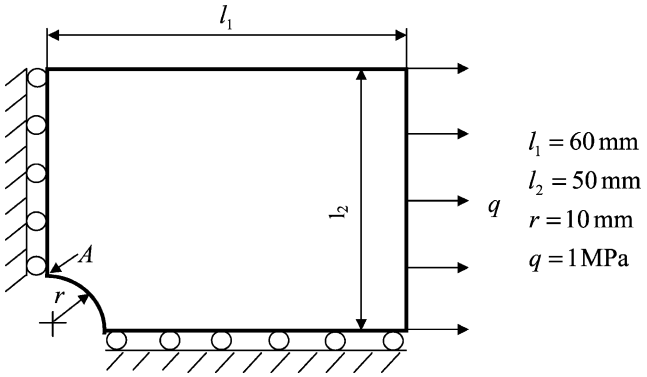

Fig. 7. Quarter of a rectangular plate containing a centered circular hole subjected to normal tension.

double precision real-arithmetic. The corresponding flow chart of the algorithm is shown in Fig. 4.

3. Examples

To illustrate the visualization flexibility and accuracy of the modified IMFM, following two examples are considered. The cloud data obtained of Mises equivalent stress with 30 colors are depicted in Figs. 6 and 8.

In all the calculations, linear elasticity with Young's modulus $E = 2.1 \times 10^5$ MPa and Poisson's ratio $\nu = 0.3$ are assumed.

3.1. A hollow cylinder subjected to internal pressure

Owing to the symmetry of the problem only one quadrant of the cylinder is analyzed (see Fig. 5).

The HT FE model of this plane strain problem consists of 32 C2D4T elements and 45 nodes. It can be observed from Fig. 6(a) that the color of the cloud data changes transitionally from blue on the inner cylinder surface to yellow on the outer cylinder surface. This indicates that Mises equivalent stresses of the domain under consideration drop from the maximum to the minimum gradually. For comparison, the corresponding analytical solution is also plotted in Fig. 6(b). The form and the trend of the contours are the same for both methods, but the HT FE model produces some corners in the contours. Nonetheless, the present approach may predict the reliable information of stress distribution in certain extent.

3.2. A rectangular plate containing a hole under uniaxial tension

Only one quarter of the rectangular plate with a centered circular hole and deformation under plane stress conditions is considered, due to its geometry and load symmetry.

Using the HT FE model, the solution domain is discretized with 44 C2D8T elements and 163 nodes. The corresponding cloud data is illustrated in Fig. 8(a). According to the theory of elasticity [20], stress concentration exists at point A of Fig. 7. As can be evidently observed from Fig. 8(a), it is blue in the vicinity of point A. This fact explains that the cloud data of the plate reflects the local effect of this problem. Similarly as done in the former example, the analytical data are provided in Fig. 8(b) for verification purpose. The comparison shows that the Mises equivalent stress distribution obtained by the modified IMFM agrees with the analytical solution on the whole, although there are some discrepancies in the figures.

4. Conclusions and discussion

The method presented was developed for visualizing the results obtained from ABAQUS user-defined HT FE models. Two examples have been examined, and the corresponding cloud data demonstrate the reliability, efficiency and robustness of the computational algorithm. The aim of the technique based on modified IMFM is to display a graphical representation of the post-processing results of HT FEM and to develop a customized visualization software for non-standard numerical methods.

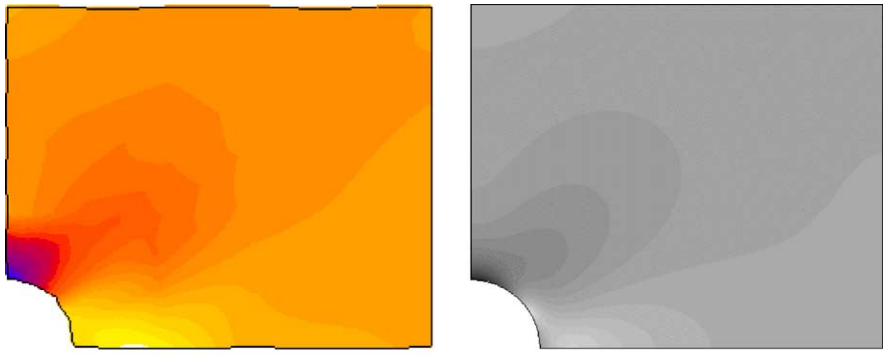

(a) Modified IMFM solution (b) Analytical solution

Fig. 8. Cloud data of Mises equivalent stress for the plate with a circular hole.

The modified IMFM is obviously simple from a computational point of view, in respect of both programming and computation time. It is important to note that the approach described is valid for various types of element.

At present, the coded VC++ program can display cloud data of uniform contour intervals only. Extension to the case of continuous cloud data is possible. Furthermore, it is also straightforward to generalize the modified IMFM to 3D cases if we distinguish each surface of 3D HT finite elements before scanning it, and consider each surface as a 2D problem.

References

[1] Jirousek J, Leon N. A powerful finite element for plate bending. Comput Meth Appl Mech Eng 1977;12:77–96.

[2] Piltner R. Special finite elements with holes and internal cracks. Int J Numer Meth Eng 1985;21:1471–85.

[3] Stelzer JF, Welzel R. Plotting of contours in a natural way. Comput Struct 1987;24:1757–69.

[4] Meek JL, Beer G. Contour plotting of data using element isoparametric representation. Int J Numer Meth Eng 1976;10:954–7.

[5] Akin JE, Gray MH. Contouring on isoparametric surfaces. Int J Numer Meth Eng 1977;11:1893–7.

[6] Gray MH, Akin JE. An improved method for contouring on isoparametric surfaces. Int J Numer Meth Eng 1979;14:451–72.

[7] Yeo MF. An interactive contour plotting program. Eng Comput 1984; 1:273–9.

[8] Soriano HL, Lima SS. A method for graphic stress representation. Comput Struct 1997;63:1223–8.

[9] Wang KP, Bruch Jr JC. Adaptive quadtree subdividing contour plotting algorithms. Eng Comput 1995;12:545–53.

[10] Singh C, Sarkar D. Simple and fast algorithm for the plotting of contours using quadrilateral meshes. Finite Elem Anal Des 1990;7: 217–28.

[11] Gopalakrishnan TC, Korttom M. Algorithm for contouring and interpolation of data using bilinear finite elements. Finite Elem Anal Des 1993;14:37–54.

[12] Rajasekaran S, Venkatesan KG. New contouring algorithm. Comput Struct 1995;54:953–77.

[13] Sun WL, Yang WS, Man ZQ. An algorithm to display data in the post-processing of finite element. J Harbin Univ Sci Technol 2000;5: 77–80.

[14] Jia AC, Han CC, Wei XP. Multiple-section cloud picture display of analysis data of dam seismic response. J Dalian Univ Technol 2001; 41:372–5.

[15] Nikishkov GP. Generating contours on FEM/BEM higher-order surfaces using Java 3D textures. Adv Eng Software 2003;34: 469–76.

[16] Ma SY, Wang KY, Fu SH. Technique of cloud picture display in post-processing of FEM—isoparametric mapping method. J Hebei Univ Technol 2003;32:23–8.

[17] Qin QH. The Trefftz finite and boundary element method. Southampton: WIT Press; 2000.

[18] Jirousek J, Venkatesh A. Hybrid Trefftz plane elasticity elements with p-method capabilities. Int J Numer Meth Eng 1992;35: 1443–72.

[19] Guo XX, Liu JS. Development of dynamic cloud chart in post-processing of finite element for metal forming. Chin J Forging Tech 2000;5:13–15.

[20] Xia ZG, Jiang LP, Tang SG. Elastic mechanics and its numerical methods. Shanghai: Tongji University Press; 1997.